Title

Electric Double-Layer Structure in Primitive Model Electrolytes: Comparing Molecular Dynamics with Local-Density Approximations

Journal

Langmuir, 31(11)

ISSN

0743-7463

Authors

Giera, Brian
Henson, Neil
Kober, Edward M
et al.

Publication Date

2015-03-24

DOI

10.1021/la5048936

Peer reviewed

Langmuir

Article

pubs.acs.org/Langmuir

Electric Double-Layer Structure in Primitive Model Electrolytes: Comparing Molecular Dynamics with Local-Density Approximations

Brian Giera,[†,‡] Neil Henson,[§] Edward M. Kober,[§] M. Scott Shell,[†] and Todd M. Squires*[,†]

[†]Department of Chemical Engineering, University of California—Santa Barbara, Santa Barbara, California 93106, United States

[‡]Lawrence Livermore National Laboratory, Livermore, California 94551, United States

[§]Los Alamos National Laboratory, Los Alamos, New Mexico 87545, United States

ABSTRACT: We evaluate the accuracy of local-density approximations (LDAs) using explicit molecular dynamics simulations of binary electrolytes comprised of equisized ions in an implicit solvent. The Bikerman LDA, which considers ions to occupy a lattice, poorly captures excluded volume interactions between primitive model ions. Instead, LDAs based on the Carnahan—Starling (CS) hard-sphere equation of state capture simulated values of ideal and excess chemical potential profiles extremely well, as well as the relationship between surface charge density and electrostatic potential. Excellent agreement between the EDL capacitances predicted by CS-LDAs and computed in molecular simulations is found even in systems where ion correlations drive strong density and free charge oscillations within the EDL, despite the inability of LDAs to capture the oscillations in the detailed EDL profiles.

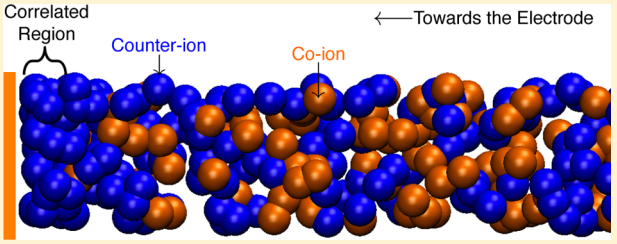

1. INTRODUCTION

Electric double-layers (EDLs) form adjacent to charged surfaces in electrolytes, regardless of whether the charge is fixed (e.g., via charged surface groups or specific ion adsorption) or arises due to an externally applied electrostatic potential (e.g., on an electrode). Ions in the electrolyte rearrange to screen this interfacial charge over a length scale that is determined by the characteristics of the electrolyte. EDLs play a central role in colloidal[1] and polyelectrolyte science,[2] micro- and nanofluidics,[3] surface conductivity,[4] "blue energy" systems,[5] and in electric double-layer capacitors[6] that store energy electrochemically across the EDL. Detailed ion density profiles within EDLs have been measured experimentally using various techniques and materials,[7] e.g., from X-ray reflectivity measurements of liquid—liquid interfaces[8,9] and Langmuir monolayers.[10] Rational design and engineering of EDL capacitors,[11] electrokinetic flows,[12] or capacitive deionization systems[13−15] require accurate double-layer models of electrolytic and ionic liquid systems.[7,16]

Models and simulations have been developed to interpret and predict EDL structure and capacitance. Simple mean-field approaches remain popular because they are relatively easy to use, yet they still capture essential EDL properties. The most widely used are local-density approximations (LDAs),[17] which assume that ions interact with mean fields (electrostatic or steric) rather than explicit ion—ion interactions. By nature, LDAs neglect nonlocal correlations between ions and can therefore fail at large potentials or in concentrated electrolytes, both of which are experimentally relevant.[1,18] As described by Gillespie in a recent review,[19] they can also fail on more basic theoretical grounds near interfaces or electrodes if locally averaged concentrations are not used, where the averaging is performed over an ion-sized volume. Despite these well-known shortcomings, LDA models have been proposed to treat short-ranged enthalpic[20] and steric interactions between equisized[21,22] and asymmetric[23] ions for ionic liquids,[24] electrochemical cells,[6,13] and liquid—liquid interfaces.[8,10]

We recently showed that all EDLs described by any particular LDA have self-similar scaling and thus collapse onto a single master curve when plotted against suitably derived similarity coordinates.[25] Such similarity coordinates can be derived directly from experimentally or computationally determined EDL profiles, without assuming any particular form for a LDA. This model-free test reveals whether it is possible for any LDA to successfully describe a particular EDL and therefore whether there is any sense in attempting to identify an appropriate LDA. Nonetheless, the procedure gives no information regarding which LDA would be appropriate.

In what follows, we compare the most common LDAs against extensive molecular dynamics (MD) simulations, which explicitly treat both electrostatic and steric interactions between ions. In particular, the neglect of steric interactions between ions has long been known to yield aphysical predictions near highly charged walls and/or concentrated electrolytes.[17] Our MD simulations employ a variant of the so-called primitive model (PM), treating ions as charged Weeks—Chandler—Andersen[26] spheres in an implicit solvent. We compare MD results with predictions from the Bikerman[21] (Bik) and Carnahan—Starling[27] (CS) LDAs, each of which accounts for finite ion size in a continuum solvent by introducing an excess

Received: December 17, 2014
Revised: February 16, 2015

DOI: 10.1021/la5048936
Langmuir XXXX, XXX, XXX−XXX

term to the chemical potential of each ion. In particular, the CS-LDA treats ions as comprising a structureless hard-sphere fluid, via the Carnahan−Starling equation of state.[27] The Bik-LDA, on the other hand, assumes ions to occupy a lattice, wherein each site is occupied either by an ion or by solvent, such that solvent is increasingly displaced by ions at large surface charge densities.[17,24] Because the Bik-LDA can be solved analytically yet qualitatively captures the effect of ion saturation, it remains one of the most popular LDAs.

Although both Bik- and CS-LDA capture qualitative features of ion crowding within the EDL, quantitative assessments of the accuracy of their approximations require explicit comparison with atomistic simulations or, ultimately, experiments. We find the CS equation of state accurately predicts the excess components of the chemical potential, as measured directly in our PM simulations, over a wide range of electrolytes and volume fractions over substantial portions of all EDLs. By contrast, the Bik-LDA performs rather poorly, even qualitatively, in capturing MD results. Consequently, the CS-LDA outperforms the Bik-LDA (and, obviously, the Gouy−Chapman LDA that does not account for steric interactions at all) in predicting integrated quantities like EDL capacitance as well as local quantities like charge density profiles and components of the chemical potential.

LDAs permit only monotonic density profiles[28] and thus fail to capture the oscillatory density profiles that arise when ions pack at high concentrations. We define and measure a correlation length, l_{cor}, to parametrize the breakdown of the LDA approximation in our simulated EDLs. Beyond the l_{cor}-thick correlated layer, nonlocal effects are negligible, whereupon the CS-LDA accurately predicts PM EDL profiles over a wide range of electrode charge densities and bulk volume fractions. Somewhat surprisingly, the CS-LDA captures the EDL capacitance well, even in cases where significant density oscillations appear in the MD simulations. Thus, while the CS-LDA fails to describe (oscillatory) EDL structures in highly concentrated regions of the EDL, it nonetheless captures mean and integrated quantities associated with the EDL quite well.

2. ELECTRIC DOUBLE-LAYER MODELS

We start by reviewing salient features of the two complementary approaches to treating EDLs: explicit molecular dynamics and mean-field approximations. In what follows, both approaches treat the solvent implicitly and consider EDLs that are fully charged. LDAs assume ions to interact via average, mean-field interactions rather than with other ions individually. They account for steric (and other) interactions by incorporating physically motivated chemical potentials that depend on local quantities alone, neglecting, e.g., explicit ion−ion correlations.[17] Molecular simulations, on the other hand, account explicitly for interactions between each pair of ions at each time step and can thus naturally capture size-induced and/or electrostatic correlations among ions with pairwise interaction potentials.

2.1. Mean-Field Local-Density Approximations. Local-density approximations require the chemical potential of each ion species at every point in space $\mathbf{r}$ to depend *only* on local quantities such as the density of ions $n^{\pm}(\mathbf{r})$ or electrostatic potential $\phi(\mathbf{r})$, via

$$\mu^i_{\mathrm{LDA}}(\mathbf{r}) = \mu^i_*(T) + k_{\mathrm{B}}T \ln n^i + q^i e\phi + \mu^i_{\mathrm{ex}} \tag{1}$$

where k_{B} is the Boltzmann constant, T is temperature, q^i is ion valence, and e is the elementary charge. Equation 1 expresses the LDA chemical potential μ^i_{LDA} in terms of a standard chemical potential μ^i_*, an ideal component, a contribution from the mean electrostatic field ϕ, and an (as-yet undetermined) excess chemical potential μ^i_{ex}, respectively. Far from the surface ($\mathbf{r}\rightarrow \mathbf{r}_{\mathrm{B}}$), all quantities assume constant (bulk) values, to give

$$\mu^i_{\mathrm{LDA}}(\mathbf{r}\rightarrow \mathbf{r}_{\mathrm{B}}) \rightarrow \mu^i_{\mathrm{B}} = \mu^i_*(T) + k_{\mathrm{B}}T \ln n^i_{\mathrm{B}} + q^i e\phi_{\mathrm{B}} + \mu^i_{\mathrm{ex,B}} \tag{2}$$

Subtracting eq 2 from eq 1 gives a relative chemical potential, which we normalize by the thermal energy scale $k_{\mathrm{B}}T$ to give

$$\tilde{\mu}^i_{\mathrm{LDA}}(\mathbf{r}) = \frac{\mu^i_{\mathrm{LDA}} - \mu^i_{\mathrm{B}}}{k_{\mathrm{B}}T} = \ln \tilde{n}^i + q^i\tilde{\phi} + \tilde{\mu}^i_{\mathrm{ex}} \equiv 0 \tag{3}$$

In eq 3, the ion number density n^i has been nondimensionalized by the bulk value n^i_{B}

$$\tilde{n}^i = \frac{n^i}{n^i_{\mathrm{B}}} \tag{4}$$

and electrostatic potentials have been nondimensionalized by the thermal potential to give

$$\tilde{\phi} = \frac{\phi - \phi_{\mathrm{B}}}{\phi_{\mathrm{T}}} \tag{5}$$

where

$$\phi_{\mathrm{T}} = \frac{k_{\mathrm{B}}T}{q^i e} \tag{6}$$

In what follows, we consider symmetric electrolytes, wherein ions have identical sizes, equal and opposite valence $q^{\pm} = \pm q$, and an electroneutral bulk (for which $\phi_{\mathrm{B}} = 0$ and with $n^+_{\mathrm{B}} = n^-_{\mathrm{B}} = n_{\mathrm{B}}$ so that $\mu^+_{\mathrm{ex,B}} = \mu^-_{\mathrm{ex,B}} = \mu_{\mathrm{ex,B}}$). The bulk values $\mu^{\pm}_{\mathrm{B}}$ of the total chemical potential for each ion species are thus equal

$$\mu^{\pm}_{\mathrm{B}} = \mu_{\mathrm{B}} \tag{7}$$

Using eq 3, we solve for the free charge density

$$\rho = e(q^+n^+ + q^-n^-) = qen_{\mathrm{B}}(\mathrm{e}^{-(\tilde{\mu}^+_{\mathrm{ex}}+\tilde{\phi})} - \mathrm{e}^{-(\tilde{\mu}^-_{\mathrm{ex}}-\tilde{\phi})}) \tag{8}$$

which, when nondimensionalized by $2qen_{\mathrm{B}}$, is given by

$$\tilde{\rho} = \frac{\rho}{2qen_{\mathrm{B}}} = \frac{1}{2}(\mathrm{e}^{-(\tilde{\mu}^+_{\mathrm{ex}}+\tilde{\phi})} - \mathrm{e}^{-(\tilde{\mu}^-_{\mathrm{ex}}-\tilde{\phi})}) \tag{9}$$

LDA models for electric double layers use Poisson's equation to relate the electrostatic potential to the free charge density established by the ions. When nondimensionalized, as in eqs 5 and 9, Poisson's equation becomes

$$\lambda_{\mathrm{D}}^2\nabla^2\tilde{\phi} = -\tilde{\rho} \tag{10}$$

The Debye length λ_{D}

$$\lambda_{\mathrm{D}} = \frac{1}{\sqrt{8\pi\lambda_{\mathrm{B}}n_{\mathrm{B}}}} \tag{11}$$

naturally arises and gives a characteristic length scale over which the electrolyte screens the surface charge. Equation 11 expresses λ_{D} in terms of the Bjerrum length

$$\lambda_{\mathrm{B}} = \frac{(qe)^2}{4\pi\varepsilon k_{\mathrm{B}}T} \tag{12}$$

DOI: 10.1021/la5048936
Langmuir XXXX, XXX, XXX−XXX

which represents the distance at which the thermal energy scale k_BT balances the electrostatic energy between ions in a uniform continuum with permittivity ε. We nondimensionalize all lengths by λ_D unless otherwise indicated.

Using ρ as given by the equilibrium relation eq 8 in Poisson's equation, eq 10 gives the general modified Poisson−Boltzmann equation

$$\lambda_D^2\nabla^2\tilde{\phi} = \tilde{\nabla}^2\tilde{\phi} = \frac{1}{2}(e^{-(\tilde{\mu}_{ex}^- - \tilde{\phi})} - e^{-(\tilde{\mu}_{ex}^+ + \tilde{\phi})}) \tag{13}$$

Closing the LDA description requires a form for the excess chemical potentials $\tilde{\mu}_{ex}^{\pm}$, after which the LDA equations can be solved self-consistently by imposing constraints on the electrostatic potential at the charged interface

$$\tilde{\phi}(0) = \tilde{\phi}_0 \tag{14}$$

and in the bulk

$$\tilde{\phi}(\tilde{z}_B) = \tilde{\phi}_B \equiv 0 \tag{15}$$

Equations 3 and 8 are fairly general and can be modified for electrolytes with additional species or to incorporate nonlocal excess terms that account for ion−wall interactions, such as a wall excess chemical potential contribution $\mu^{w}{}_{ex}(z)$.[29]

The classic Poisson−Boltzmann equation describes the simplest mean-field LDA model and assumes ideal, point-like ions in a structureless continuum solvent. In this idealized limit, the excess terms in eq 1 vanish to give an ideal electrochemical potential

$$\tilde{\mu}_{GC}^{\pm} = \ln\tilde{n}^{\pm} \pm \tilde{\phi} \equiv 0 \tag{16}$$

so that ions follow a direct Boltzmann distribution, $\tilde{n}^{\pm} = \exp(\mp\tilde{\phi})$, whereupon eq 13 reduces to the (nonlinear) Poisson−Boltzmann equation

$$\tilde{\nabla}^2\tilde{\phi} = \sinh\tilde{\phi} \tag{17}$$

The Gouy−Chapman (GC) solution satisfies the nonlinear Poisson−Boltzmann equation for planar surfaces at arbitrary surface potential.[30,31] The potential drop across a GC EDL is related to the surface charge Σ according to

$$\tilde{\Sigma}_{GC} = \frac{\Sigma_{GC}}{\Sigma_{ref}} = 2\sinh\left(\frac{\tilde{\phi}_0}{2}\right) \tag{18}$$

where we have scaled surface charge density by the natural scale

$$\Sigma_{ref} = 2qen_B\lambda_D = \frac{qe}{4\pi\lambda_B\lambda_D} \tag{19}$$

Equation 17 can be linearized in the limit of low potentials ($\tilde{\phi} \ll 1$)

$$\tilde{\nabla}^2\tilde{\phi} = \tilde{\phi} \tag{20}$$

giving the Debye−Hückel (DH) EDL with potential

$$\tilde{\phi}_{DH} = \tilde{\phi}_0\exp(-\tilde{z}) \tag{21}$$

and surface charge

$$\tilde{\Sigma}_{DH} = \tilde{\phi}_0 \tag{22}$$

When the bulk electrolyte is dilute, all LDAs reduce to the DH form sufficiently far from the surface, even for highly charged electrodes.[28]

Despite its near-ubiquitous use, the GC-LDA (and eq 17 more generally) has long been known to fail for various reasons. Boltzmann-distributed densities grow exponentially with $\tilde{\phi}$ and can yield volume fractions exceeding close packing of finite-sized ions at reasonable potentials.[21,22] The point-like ion assumption can be relaxed, while remaining within the LDA framework, by incorporating an excess chemical potential that accounts for steric interactions between ions. In what follows, we consider equisized ions of diameter σ and excess chemical potentials that depend on the local volume fraction of ions Φ

$$\Phi(\mathbf{r}) = \frac{\Phi_B}{2}\left(\frac{n^+ + n^-}{n_B}\right) = \frac{\Phi_B}{2}(\tilde{n}^+ + \tilde{n}^-) \tag{23}$$

which approaches a constant bulk value, given by

$$\Phi_B = \frac{\pi}{3}n_B\sigma^3 \tag{24}$$

The Bikerman LDA (Bik-LDA) adopts a mean-field lattice-gas model for the EDL, where at most one ion can occupy each lattice site,[21] with empty sites representing implicit solvent. The Bikerman excess chemical potential

$$\frac{\mu_{ex}^{Bik}}{k_BT} = -\ln(1-\Phi) \tag{25}$$

is derived from the configurational degeneracies of non-overlapping ions among available lattice sites.[24] At sufficiently high potentials, lattice sites saturate with counterions.[22] Following eqs 2 and 3, the Bikerman chemical potential is expressed relative to its bulk value to give the dimensionless relation

$$\tilde{\mu}_{Bik}^{\pm} = \ln\tilde{n}^{\pm} \pm \tilde{\phi} + \ln\left(\frac{1-\Phi_B}{1-\Phi_B(\tilde{n}^+ + \tilde{n}^-)/2}\right) \equiv 0 \tag{26}$$

Equation 26 can be solved for $\tilde{n}^{\pm}$ to reveal a Fermi−Dirac (instead of a Boltzmann) form for the density dependence on electrostatic potential. The Bikerman free charge density is inserted into eq 10 to obtain

$$\tilde{\nabla}^2\tilde{\phi} = \frac{\sinh(\tilde{\phi})}{1 + 2\Phi_B\sinh^2(\tilde{\phi}/2)} \tag{27}$$

The capacitance relationship between surface charge and potential drop across the EDL is given for the Bik-LDA by

$$\tilde{\Sigma}_{Bik} = \sqrt{\frac{2}{\Phi_B}\ln[1 + 2\Phi_B\sinh^2(\tilde{\phi}_0/2)]} \tag{28}$$

In the case of point-sized ions, $\Phi_B \to 0$ and eqs 26−28 recover the GC-LDA and Poisson−Boltzmann eq 17.

More accurate models for excluded volume contributions to the bulk chemical potential frequently rely on integral equation expansions of a homogeneous hard-sphere fluid.[32,33] The Carnahan−Starling (CS) equation of state[27] is an accurate approximation[34] that combines the hard-sphere equations of state from the virial and compressibility routes[35] to obtain

$$\frac{\mu_{ex}^{CS}}{k_BT} = \frac{\Phi(8 - 9\Phi + 3\Phi^2)}{(1-\Phi)^3} \tag{29}$$

DOI: 10.1021/la5048936
Langmuir XXXX, XXX, XXX−XXX

The ideal and electrostatic chemical potentials and eq 29 are expressed relative to the bulk to obtain the dimensionless total CS-LDA chemical potential[17,36]

$$\tilde{\mu}_{CS}^{\pm} = \ln \tilde{n}^{\pm} \pm \tilde{\phi} + \frac{\Phi(8 - 9\Phi + 3\Phi^2)}{(1-\Phi)^3} - \frac{\Phi_B(8 - 9\Phi_B + 3\Phi_B^2)}{(1-\Phi_B)^3} \equiv 0 \tag{30}$$

To solve the CS-LDA, just as with all LDAs, each ion distribution is determined by solving each chemical potential expression in eq 30: $\{\tilde{\mu}_{CS}^{+},\tilde{\mu}_{CS}^{-} = 0,0\}$. While this can be done analytically for the Bik-LDA, it must be done numerically for the CS-LDA. Nonetheless, the free charge density can then be determined and used in eq 10 to determine $\tilde{\rho}_{CS}(\tilde{\phi})$. Both CS- and Bik-LDA recover the GC limit as $\Phi_B \to 0$ when the excess chemical potential vanishes.

Charge−voltage curves are relatively straightforward to measure, and the capacitance is important in various electrochemical energy storage devices. The functional relationship between the surface charge density and the applied potential $\tilde{\phi}_0$ across the EDL, from which the capacitance follows naturally, can be obtained for any LDA[17]

$$\tilde{\Sigma}_{LDA}(\tilde{\phi}_0) = \mathrm{sgn}(\tilde{\phi}_0)\sqrt{-2\int_0^{\tilde{\phi}_0} \tilde{\rho}_{LDA}(\hat{\phi})\, d\hat{\phi}} \tag{31}$$

The integral, or total, capacitance is given by $\tilde{\Sigma}_{LDA}/\tilde{\phi}_0$, and the differential capacitance, by $d\tilde{\Sigma}_{LDA}/d\tilde{\phi}_0$. In what follows, however, it will become clear that charge−potential curves (eq 31) effectively integrate out spatial oscillations in ion density profiles and can thus hide discrepancies between the predictions of LDAs and molecular simulations.

2.2. Molecular Dynamics Simulations of Primitive Model Electrolytes. The primitive model is the simplest model to incorporate finite ion sizes into electrolyte dynamics, by treating ions as hard-spheres with diameter σ and valence q in an implicit solvent between uniformly charged plates. In this work, we use molecular dynamics simulations of the PM EDL in the canonical ensemble, where the number of ions N, volume V, and temperature T are held constant.

The potential energy of ions depends on pairwise ion−ion interactions and single-body ion−wall interactions. The reduced Coulomb potential

$$\tilde{U}_{Coulomb}(r) \equiv \frac{U_{Coulomb}(r)}{k_B T} = \mathrm{sgn}(q^i q^j)\frac{\lambda_B}{r} \tag{32}$$

describes the electrostatic interaction between point charges separated by distance r. To lessen numerical difficulties associated with hard-sphere repulsions, we employ the repulsive Weeks−Chandler−Andersen[26] (WCA) potential

$$\tilde{U}_{WCA}(r) = \begin{cases} \tilde{\epsilon}_{WCA}\left[\dfrac{(\sigma^6 - r^6)^2}{r^{12}}\right] & \text{if } r \le \sigma \\ 0 & \text{if } r > \sigma \end{cases} \tag{33}$$

to account for finite-size effects between ions. A characteristic repulsive interaction, described by energy scale $\tilde{\epsilon}_{WCA} = \epsilon_{WCA}/k_B T$, penalizes ions separated by less than the WCA diameter σ. As with hard-sphere systems, WCA ions separated by more than σ do not interact. The WCA diameter σ is not, strictly speaking, equivalent to a hard-sphere diameter. Instead, we will determine an effective hard-sphere diameter, as described below.

The very steep WCA potential dictates an effective minimum interion separation distance $r^{min} \sim O(\sigma)$. Therefore, the dominant contributions to pairwise interactions depend on the relative magnitudes of λ_B and σ. Choosing $\lambda_B \ll \sigma$, as we do here, ensures that strong ion−ion interactions are predominantly steric in nature rather than electrostatic. As a result, ions remain dissolved (i.e., do not aggregate or precipitate out of solution), and any non-mean-field correlations arise due to steric, rather than electrostatic, interactions.

As described above, two length scales appear naturally in any electrolyte: the Debye screening length λ_D (eq 11), which depends on ion concentration, and the Bjerrum length (eq 12), which depends upon ion valence. These two length scales, in turn, specify the surface charge density scale Σ_{ref}. Finite ion diameters σ introduce another dimensionless parameter, the bulk volume fraction Φ_B (eq 24), which can be expressed in the form

$$\Phi_B = \frac{\sigma^3}{24\lambda_B\lambda_D^2} \tag{34}$$

Nondimensionalizing all lengths by λ_D, then, reveals any PM EDL to be characterized uniquely by four dimensionless parameters: Φ_B, λ_B/λ_D, Σ/Σ_{ref}, and $\tilde{\epsilon}_{WCA}$. Appreciable dependence is seen only for the three parameters Φ_B, λ_B/λ_D, and Σ/Σ_{ref}, as simulations show significant insensitivity to $\tilde{\epsilon}_{WCA}$, so long as it is $O(1)$ or greater, as we take throughout this work.

Steric repulsions between ions and electrodes depend only on the distance from walls. The electric field term

$$\tilde{U}_{field}(\tilde{z}) = -q^i\tilde{\Sigma}\tilde{z} \tag{35}$$

accounts for the potential energy ions experience between two walls with equal and opposite surface charge density. The wall potentials are the repulsive part of the 9-3 potential,[37] analogous to the WCA interaction used between ions

$$\tilde{U}_w^{+}(\tilde{z}) = \begin{cases} \dfrac{\epsilon_w}{k_B T}\sqrt{\dfrac{5}{18}}\left[\left(\dfrac{\delta_w}{\tilde{z}\lambda_D}\right)^9 - 3\left(\dfrac{\delta_w}{\tilde{z}\lambda_D}\right)^3 + 2\right] & \text{if } \tilde{z} \le \delta_w/\lambda_D \\ 0 & \text{if } \tilde{z} > \delta_w/\lambda_D \end{cases} \tag{36}$$

and

$$\tilde{U}_w^{-}(\tilde{z}) = \begin{cases} 0 & \text{if } \tilde{z} < L/\lambda_D \\ \dfrac{\epsilon_w}{k_B T}\sqrt{\dfrac{5}{18}}\left[\left(\dfrac{\delta_w}{\delta_w + L - \tilde{z}\lambda_D}\right)^9 - 3\left(\dfrac{\delta_w}{\delta_w + L - \tilde{z}\lambda_D}\right)^3 + 2\right] & \text{if } \tilde{z} \ge L/\lambda_D \end{cases} \tag{37}$$

with characteristic energy ϵ_w and wall thickness parameter δ_w.

3. METHODS

We perform MD simulations between walls separated by a distance L, with 2D periodicity in the transverse directions, using LAMMPS[38] to compute primitive model electric double layers. Periodic dimensions and wall separations L are chosen to exceed all other length scales so that they do not impact computation results. The system is maintained at constant temperature with a Langevin thermostat.[39] Charge-centered WCA ions of diameter $(0.001 \le \sigma/L \le 0.0122)$ and

DOI: 10.1021/la5048936
Langmuir XXXX, XXX, XXX−XXX

characteristic energy $\epsilon_{WCA} = k_B T$ are confined between two repulsive walls with uniform charge density $\pm\Sigma$, thickness $\delta_w = L/500$, and characteristic energy $\epsilon_w = k_B T$ (eqs 32−37). We evaluate the Coulomb potential with a particle−particle particle−mesh slab Ewald sum[40] with the default accuracy of 10^{-4}. For each PM electrolyte (specified by $\{\Phi_B; \lambda_B/\lambda_D; \tilde{\epsilon}_{WCA}\}$) and equal and opposite surface charge densities $\pm\tilde{\Sigma}$, we equilibrate $O(800-1400)$ ions for 5 M time steps and then collect 50 k snapshots over 50 M steps, requiring 50−100 CPU hours per run. By averaging over bins of width λ_D (i.e., a nondimensional thickness of 1), we then compute time-averaged ion densities, voltages, and spatial profiles of the excluded volume excess chemical potential using Widom insertion[41] using 250−500 M total test insertions per simulation.

In what follows, we compare CS- and Bik-LDA predictions for ion concentrations, charge densities, and chemical components with results that are computed from MD simulations of PM EDLs. To do so, we first determine an effective hard-sphere ion diameter from the WCA potentials that we have assumed. Barker et al.[33,42] match the configurational partition function for a system of particles with an arbitrary pairwise potential to a reference system of hard-spheres; they prescribe an effective hard-sphere diameter σ_{eff} from the WCA diameter σ

$$\sigma_{eff} = \int_0^{\sigma} [1 - e^{-\tilde{U}_{WCA}(\hat{r})}]\, d\hat{r} \tag{38}$$

Direct comparisons with hard-sphere simulations reveal eq 38 to deviate by $\lesssim$2%.[43] We compute σ_{eff} for eq 29 to calculate the CS-LDA. The effective size of the WCA ions we use in our simulations is essentially constant at $\sigma_{eff}/\sigma = 0.9048 \pm 10^{-5}$ for $(0.5 \le \sigma \le 6.1)$.

Previous studies that employ the Bik-LDA have chosen the lattice spacing to be given by the solvation shell diameter for ions in aqueous electrolytes,[22] from fits to experimental data,[17] or by enforcing voltage-dependent expressions to distinguish between differently sized cations and anions in the case of ionic liquids.[24] To compare with PM simulations, however, we choose the Bik-LDA diameter to match the CS-LDA results in the low-Φ limit, yielding $\sigma_{Bik} = 2\sigma_{CS}$. With this choice, Bik-LDA chemical potentials match the low-Φ simulations well (Fig 1a), but they diverge at even moderate values $\Phi \approx 0.1$. Conversely, choosing σ_{Bik} so that μ_{ex}^{EV} diverges at close packing fits simulation data very poorly everywhere. While the simplicity of the Bik-LDA admits its analytical solution, its detailed predictive capabitilities are generally quite poor. It is thus better suited for simple calculations that explore the qualitative consequences of steric interactions.

4. RESULTS AND DISCUSSION

4.1. Diffuse Electric Double-Layer Descriptions. Figure 1 shows excluded volume chemical potentials measured from 221 PM EDL simulations, wherein ion valences are chosen to span the range of weakly charged ions. Figure 1a also shows steric contributions computed from fully periodic Monte Carlo simulations of uncharged WCA particles, which explicitly exclude electrostatic correlations and wall-ordering effects. For comparison, predictions for μ_{ex}^{EV} from both CS- and Bik-LDAs are shown as a function of local packing fraction Φ within three distinct spatial regimes: in the bulk (Figure 1a), for ion−wall distances between 3σ and 6σ (Figure 1b), and within 3σ from the wall (Figure 1c). CS predictions are practically indistinguishable from values measured from MD simulations in the bulk (Figure 1a), provided we use the effective hard-sphere diameter given by eq 38. Bik-LDA, however, gives only reasonable agreement in the dilute limit ($\Phi \to 0$) and predicts a steric contribution that diverges at much lower Φ than is observed. If, by contrast, the ion size was chosen to fit the divergence, then the Bik-LDA would under predict throughout the range of Φ. In all cases, then, the CS-LDA outperforms the Bik-LDA over all volume fractions.

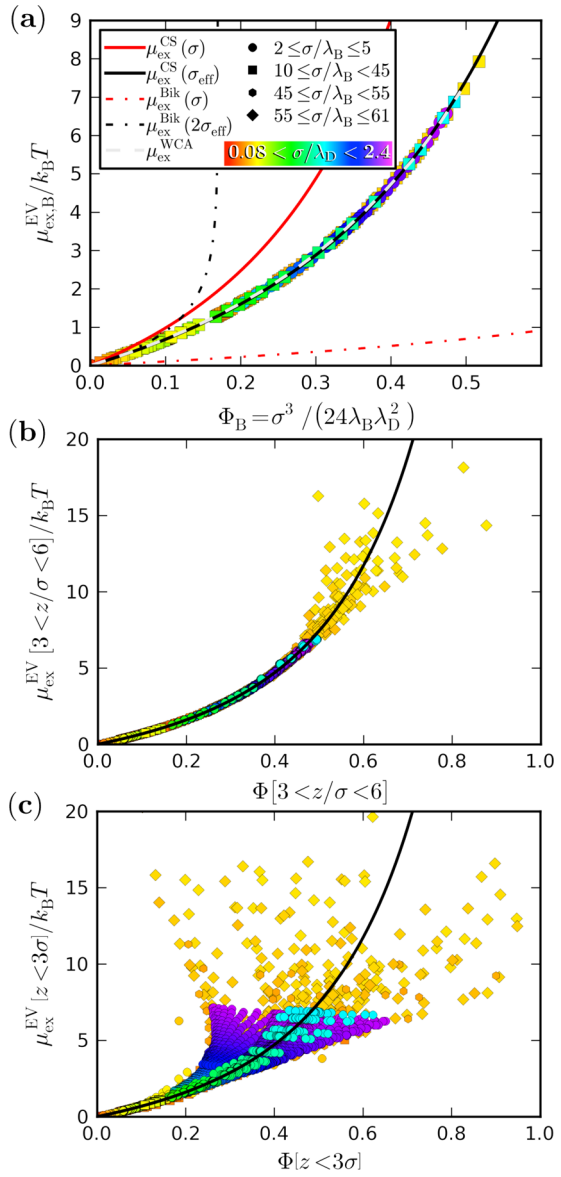

Figure 1. Local-density approximations for the excluded volume excess chemical potential and primitive model measurements from weakly and strongly charged electric double layers $0 \le \tilde{\Sigma} \le 15$. (a) Bulk measurements from PM EDLs [markers] and uncharged WCA particles [μ_{ex}^{WCA}] collapse onto the Carnahan−Starling LDA [μ_{ex}^{CS}] when using the effective hard-sphere diameter from eq 38 in eq 29. The Bikerman LDA [μ_{ex}^{Bik}] fails at all but infinitesimal volume fractions, even when determining a best fit with the effective lattice size as a free parameter. (b) Between 3 and 6 ion diameters from the electrode, CS fails to capture μ_{ex}^{EV} for $\Phi \gtrsim 0.40$ due to significant ion ordering. (c) Adjacent to the electrode, CS works only for semidilute volume fractions $\Phi \lesssim 0.10$.

Far from the electrode, PM ions interact as they would in a purely homogeneous system (Figure 1a). CS accurately describes bulk-like excluded volume interactions in both dilute and highly packed regimes. Closer to the wall, steric contributions cannot be described solely from the local volume fraction. In the intermediate region between the bulk and wall, the PM chemical potential no longer collapses onto CS due to emergent size-induced correlations at $\Phi \gtrsim 0.40$ (Figure 1b). Adjacent to the electrode, both LDAs fail dramatically beyond $\Phi \gtrsim 0.10$, where ion ordering becomes significant (Figure 1c).

DOI: 10.1021/la5048936
Langmuir XXXX, XXX, XXX−XXX

Having compared Bik- and CS-LDA models with measured excluded volume chemical potentials from PM EDLs of different ion charges, sizes, and bulk concentrations, we now turn to a closer evaluation, looking at detailed profiles of a smaller subset of simulations. Specifically, we examine weakly charged ions over a range of wall surface charge densities. We use these simulations to elucidate where and when the LDA approach breaks down for low-valence PM EDLs, which cannot approach closer than the Bjerrum length ($\sigma > \lambda_B$). We simulate 8 sets of PM EDLs, each of which has a different ion diameter σ. Eleven different surface charge densities ($0 \leq \tilde{\Sigma} < 7.1$) are simulated for each σ, yet the bulk volume fraction Φ_B is enforced to be constant for all $\tilde{\Sigma}$ simulated for each σ. Both the Bjerrum length ($\lambda_B/\lambda_D = 0.0068 \pm 0.0002$) and screening lengths ($\bar{\lambda}_D = 14.6 \pm 3\%$) were held fixed for these 88 simulations.

Figure 2 compares the surface charge density versus voltage predictions from the Debye–Hückel, Gouy–Chapman, Bikerman, and Carnahan–Starling local-density approximations against the primitive model simulation results. In the limit of small voltages (or, equivalently, low surface charge densities), capacitance curves measured from MD simulations and computed from LDAs all collapse onto the (expected) linear DH-LDA capacitance. The MD results depart from the DH, GC, and Bik-LDAs predictions once the dimensionless surface charge density $\tilde{\Sigma}$ or potential drop $\tilde{\phi}_0$ become $O(1)$. The DH and GC-LDAs, which neglect steric effects, always overpredict the capacitance of PM EDLs once the volume fraction becomes nonzero.

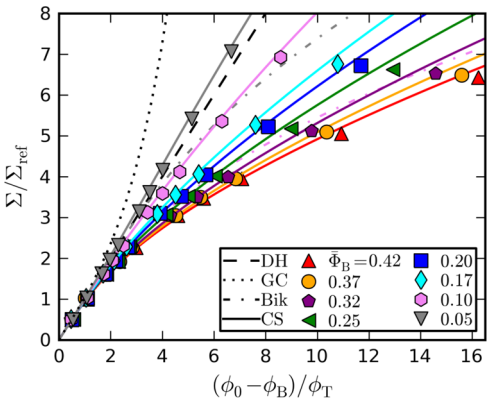

Figure 2. Surface charge density versus total potential drop from 8 sets of PM EDLs that differ in bulk volume fraction. All simulations collapse onto LDA predictions in the low charge limit $[\tilde{\Sigma},\tilde{\phi}_0] \to 0$. Beyond $\tilde{\phi}_0 \gtrsim 1$, Debye–Hückel and Gouy–Chapman diverge and Bikerman always underestimates the integrated capacitance ($\tilde{\Sigma}/\tilde{\phi}_0$), so only semidilute curves are included for clarity. Carnahan–Starling qualitatively matches PM capacitance, but it consistently gives higher values at increased charge densities and bulk volume fractions.

The Bik-LDA is better than GC in that it does not predict divergent capacitances. Instead, it underestimates the capacitance because the Bikerman excluded volume chemical potential, eq 25, grossly overpredicts measured values for μ_{ex}^{EV} (Figure 1). Over the studied range of $\Phi_B \leq 0.42$, the energy required to pack lattice ions exceeds that of spherical WCA ions. PM counterions reach higher concentrations than Bik-LDA predicts, which, in turn, leads to greater simulated capacitances at large voltages.

Capacitance curves computed using the CS-LDA, on the other hand, capture the measured MD results well even at higher $\tilde{\phi}_0$ and Φ_B, with noticeable deviations appearing for $\Phi_B = 0.37$ and 0.42. From Figure 1c, the CS-LDA accurately predicts μ_{ex}^{EV} except near the electrode where, like GC and Bikerman, it under predicts μ_{ex}^{EV} when compared with simulations. This underestimation leads the CS-LDA to slightly overpredict the capacitance of strongly charged electrodes $\tilde{\Sigma} \gtrsim 5$ and appreciable bulk volume fractions $\Phi_B \geq 0.10$.

Given how well the CS-LDA captures the total capacitance over a wide range of electrode surface charge densities and bulk volume fractions (Figure 2), we now examine the detailed spatial profiles within the EDLs, as predicted by CS-LDA and measured in PM MD simulations, for moderate and large bulk volume fractions (Figure 3). We focus on the first 10 ion diameters from the wall, beyond which the simulated and CS-LDA chemical potential profiles both converge to their bulk values. Notably, size-induced oscillations are evident in the PM simulations for both $\Phi_B = 0.17$ and 0.42, at moderate to high $\tilde{\Sigma}$. Such oscillations cannot be captured by the CS-LDA, or indeed *any* LDA model. Co-ion densities become exceedingly small, $\tilde{n}^+ \approx \exp(-10)$, near the surface, where Φ is the highest and the CS-LDA is most prone to failure. The oscillatory region for counterions is more pronounced at higher charge densities and larger bulk volume fractions. As expected from capacitance measurements (Figure 2), the CS-LDA predicts an electrostatic potential $\tilde{\phi}$ that is slightly lower than measured from PM profiles.

Figure 3a,b reveals the ideal component of the co-ion chemical potential, $\tilde{\mu}_{ideal}^{+} = \ln \tilde{n}^+$, to agree well with CS-LDA predictions, with size-induced oscillations appearing only at high volume fractions. Size-induced oscillations in the ideal counterion chemical potentials (Figure 3c,d) are much more pronounced than for co-ions, with obvious ringing even at the lowest surface potentials. Such oscillations are even stronger at higher bulk volume fractions, extending many ion diameters into the bulk. The total electrostatic potential drop, however, shows no oscillatory ringing for PM EDLs (Figure 3e,f), with surprisingly good agreement between CS-LDA and PM MD simulations. The total potential drop for a fixed $\tilde{\Sigma}$ increases with Φ_B, as excluded volume interactions force screening to occur over longer distances. Finally, the excess chemical potential due to excluded volume, measured using Widom insertion for the PM EDLs, is overpredicted by the CS-LDA at $\tilde{\Sigma} = 6.8$ for $\Phi_B = 0.17$ and at lower $\tilde{\Sigma}$ for the higher volume fraction Φ_B (Figure 3g,h).

Note that the Widom insertion technique becomes unreliable in highly concentrated regions, e.g., near highly charged walls and concentrated electrolytes, as overlapping WCA ions would require an exceedingly large number of insertions to properly average. EDLs with large packing fractions are prone to ion layering, as seen in the $\ln \tilde{n}^-$ measurements (Figure 3c,d). The general LDA approach, which neglects pairwise ion interactions, would fail to describe these highly correlated PM EDL regimes. Despite the emergence of extended correlated regions within PM EDLs, whose oscillations cannot be captured by any LDA,[25] the measured capacitance curves appear to be predicted quite well by the CS-LDA.

4.2. Characterizing Correlations. In general, spatial correlations of ions near electrodes can be due to either electrostatic or steric forces and can occur both parallel and perpendicular to the wall. Because we simulate a limited class of electrolytes with weakly charged ions, we assume Coulomb

DOI: 10.1021/la5048936
Langmuir XXXX, XXX, XXX–XXX

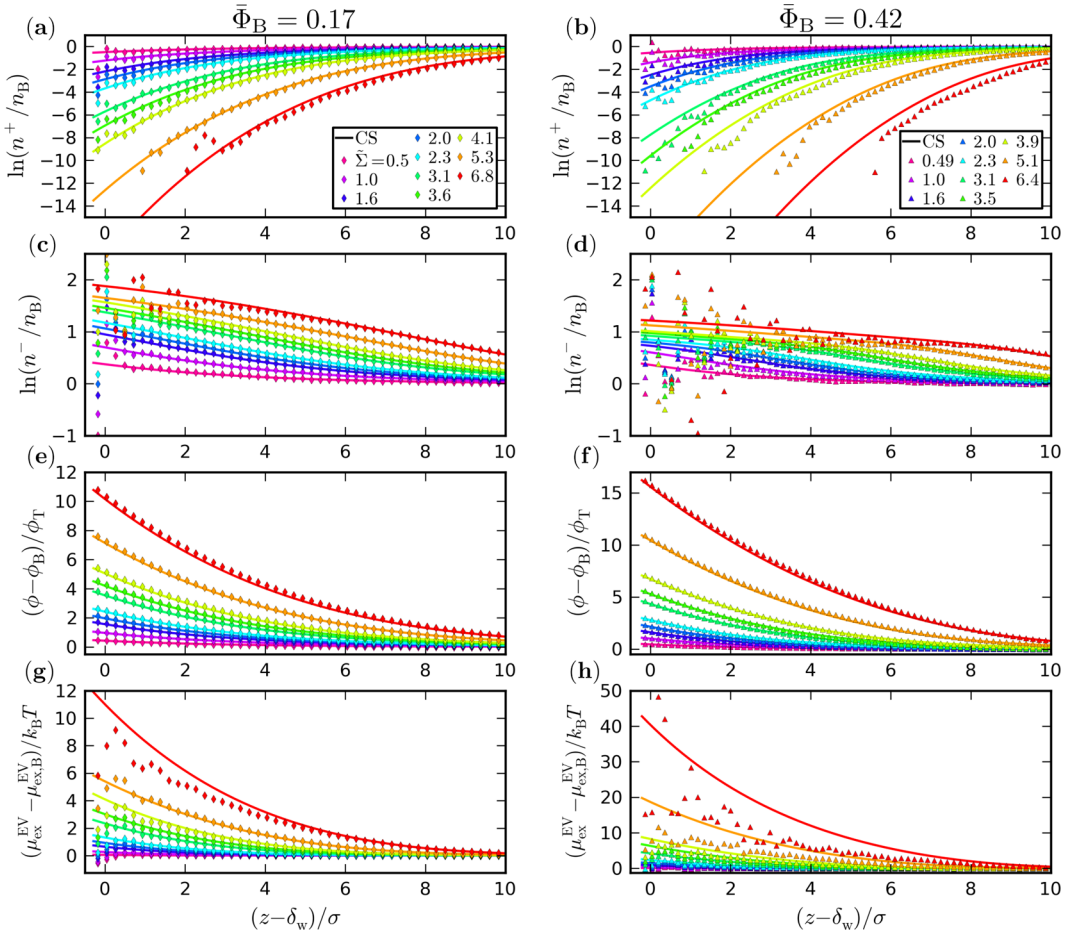

Figure 3. Individual components of the chemical potential measured from PM EDL simulations, and compared against predictions from the CS-LDA, at moderate ($\bar{\Phi}_B$ = 0.17, left column) and high ($\bar{\Phi}_B$ = 0.42, right column) bulk volume fractions. The ideal component of the chemical potentials for (a, b) co-ions, $\tilde{\mu}^+_{ideal} = \ln \tilde{n}^+$, and (c, d) counterions; (e, f) local electrostatic potential; and (g, h) excess chemical potential due to excluded volume.

correlations are negligible by comparison to size-induced correlations for PM EDLs characterized by $\lambda_B \ll \sigma$. Figure 3 reveals that even weakly-charged PM ions form correlated layers near the wall, with oscillations in the ideal and excluded chemical potential profiles that grow with increasing applied charge density and bulk volume fraction. Outside of some correlation length l_{cor} (identified below), however, CS-LDA predictions describe the PM simulations well.

There is some flexibility in defining l_{cor}; after all, the CS-LDA describes the (integrated) capacitive curves quite well. In principle, one could compare PM to LDA profiles and define l_{cor} wherever deviations exceed some meaningful threshold. However, this estimate for l_{cor} would depend upon the particular LDA that is chosen and/or some chosen threshold. Instead, we define l_{cor} to correspond to the distance beyond which oscillations in $\tilde{\rho}$ are indistinguishable from statistical bulk fluctuations. In so doing, we identify l_{cor} from simulated PM free charge density profiles in a manner that is independent of any particular LDA model.

Figure 4 illustrates the approach on PM EDLs with $\bar{\Phi}_B$ = 0.42, simulated for a range of applied surface charge densities. A quintic spline interpolant $\tilde{\rho}_{spline}$ is generated from simulated free charge density profiles, measured at 250 distinct positions. Positions $z^▲$ of extrema in $\tilde{\rho}_{spline}$ are then located numerically, by solving $d\tilde{\rho}_{spline}/d\tilde{z} = 0$. These extrema may reflect either excluded volume correlations or statistical noise. Oscillations are attributed to steric ion correlations if adjacent maxima and minima have $O(\sigma/2)$ spacing, in which case l_{cor} is found by identifying the farthest such extremum from the wall. Although no specific LDA model was used in Figure 4, l_{cor} coincides well with the onset of discrepancies between predicted (CS-LDA) and measured free charge density profiles.

We apply this algorithm to the 88 PM EDL simulations of weakly charged ions with fixed Bjerrum and screening length shown in Figure 2. A contour plot of l_{cor}, normalized by σ, as a function of Φ_B and $\tilde{\Sigma}$, appears in Figure 5. PM EDLs with low $\tilde{\Sigma}$ and Φ_B exhibit negligible correlations, whereas EDLs with large $\tilde{\Sigma}$ and Φ_B exhibit the thickest correlated regions, with correlation lengths up to 7σ, consistent with Figures 3 and 4.

Having extracted l_{cor} from PM EDLs, we now explore the properties of the correlated region. Since size-induced oscillations are the result of ion layering, the ion diameter is the appropriate characteristic length scale for the correlated region. We thus nondimensionalize Poisson's eq 10 by the ion diameter and express the potential relative to the surface potential (rather than the bulk potential $\phi_B = 0$)

$$2qen_B\left(\frac{\lambda_D}{\sigma}\right)^2\tilde{\nabla}^2\left(\frac{\phi-\phi_0}{\phi_T}\right) = -\rho_{cor} \tag{39}$$

From eq 39, we define the reduced correlated free charge density

DOI: 10.1021/la5048936
Langmuir XXXX, XXX, XXX−XXX

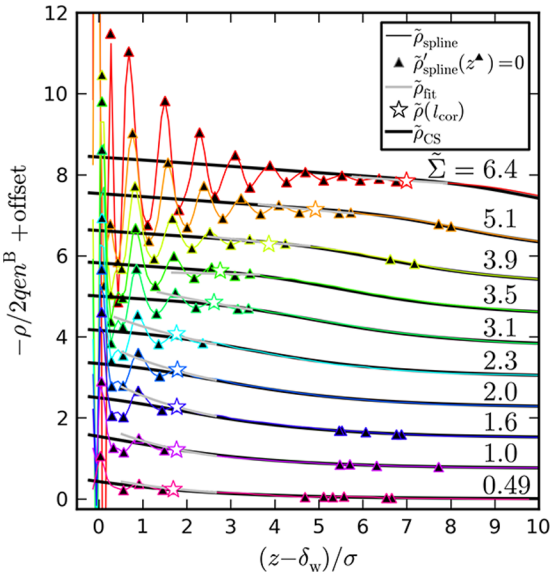

Figure 4. A model-free method to determine l_{cor} from simulated PM free charge densities with $\bar{\Phi}_B = 0.42$. We generate spline interpolants from discrete profiles, find extrema $z^{\blacktriangle}$, and identify l_{cor} (☆) by examining deviations of potentially correlated regions $\tilde{\rho}(z < z^{\blacktriangle})$ from exponential fits of bulk-like regions $\tilde{\rho}_{fit}$. Although l_{cor} appears to coincide with onset of deviations from CS-LDA profiles, this approach is independent of CS or *any* specific LDA.

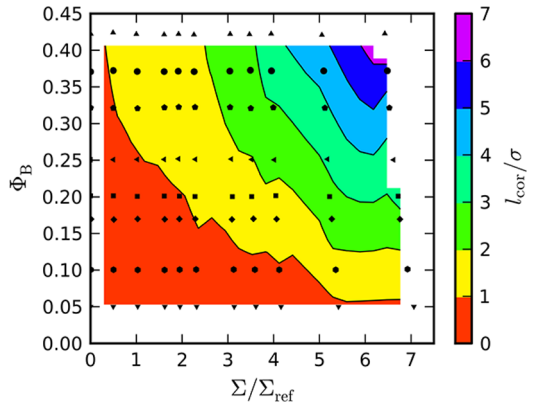

Figure 5. Contour plot of the correlation length l_{cor} measured from 88 PM EDLs, where λ_B and λ_D is held constant, using the technique described in the text and shown in Figure 4. The correlation length grows with increasing surface charge density and bulk volume fraction.

$$\tilde{\rho}_{cor} \equiv \frac{\rho_{cor}}{2qen_B}\left(\frac{\sigma}{\lambda_D}\right)^2 = \rho_{cor}\frac{\sigma^2}{\Sigma_{ref}\lambda_D} \tag{40}$$

We integrate eq 39 once to obtain the correlated surface charge

$$\tilde{\Sigma}_{cor} \equiv -\Sigma_{cor}\frac{\sigma}{\Sigma_{ref}\lambda_D} = \int_0^{l_{cor}/\sigma} \tilde{\rho}_{cor}\, d\hat{z} \tag{41}$$

and again to obtain the voltage drop across the correlated region

$$\delta\tilde{\phi}_{cor} \equiv -\left(\frac{\phi_{cor}-\phi_0}{\phi_T}\right) = \int_0^{\tilde{l}_{cor}}\left(\int_0^{\tilde{l}_{cor}} \tilde{\rho}_{cor}(\hat{s})\, d\hat{s}\right) d\hat{z} \tag{42}$$

The ratio of eqs 41 and 42 gives the integrated capacitance of the correlated EDL region.

A log−log plot of $\tilde{\Sigma}_{cor}$ vs $\Delta\tilde{\tilde{\phi}}_{cor}$ reveals the correlated EDL capacitance to collapse onto a power-law over nearly three decades of computed values (Figure 6), with a best-fit exponent

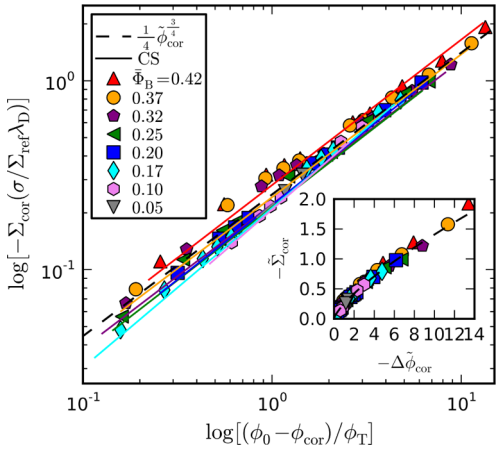

Figure 6. Surface charge density versus electrostatic potential dropped across the correlated layer of dilute and concentrated CS-LDA and PM electrolytes. CS-LDA captures the correlated capacitances at each bulk volume fraction. A best fit of data for all bulk volume fractions reveals correlated PM EDLs to follow a $^3/_4$ power law for nearly three decades of charge density and surface potential measurements.

around $^3/_4$. Somewhat surprisingly, the CS-LDA predicts the capacitance of the correlated layers, regardless of whether the PM electrolytes are semidilute, moderate, or highly concentrated. This agreement suggests that the CS-LDA describes the mean EDL behavior (i.e., the curve that would result if correlation-based oscillations were removed) so well that it can capture integrated quantities like EDL capacitance, even if it misses detailed structure.

5. CONCLUSIONS

The governing philosophy of this work has been to compare molecular simulations of EDLs formed by primitive model electrolytes (which account explicitly for pairwise ion−ion interactions) against EDLs predicted using various LDAs that have been designed to account for finite ion size. By nondimensionalizing variables in our systems, rather than working with parameters specific to a particular electrolyte, we intend for our results to be extended to a wide range of electrolytes of specific interest to future researchers. Our results span a wide variety of (dimensionless) ionic strength, ion valence, screening length, ion size, and surface charge densities.

One important, qualitative result of this work is that the Bikerman LDA, which is arguably the simplest to implement owing to its analytical tractability, is essentially incapable of capturing any quantitative features of PM EDLs. Choosing the lattice size to match the low-Φ regions of the EDL leads to predictions of premature divergences (e.g., close-packing occurs at potentials that are much too low), whereas choosing the lattice sizes to match the expected divergences (e.g., Φ at random close packing) leads to significant underestimation of steric effects at lower Φ. Such qualitative discrepancies arise due to the difference between lattice-constrained ions and hard-sphere (or hard-sphere-like) ions. The Bik-LDA, therefore, is much better suited to qualitative studies of steric effects, where analytical simplicity enables one to easily compute the

DOI: 10.1021/la5048936
Langmuir XXXX, XXX, XXX−XXX

qualitative consequences of steric repulsions rather than any quantitative predictive capabilities.

The Carnahan−Starling LDA, on the other hand, is remarkably effective at capturing many important features of PM EDLs. In particular, capacitance curves for PM and CS-LDA EDLs match extremely well, and detailed EDL profiles (e.g., of electrostatic potential, counterion and cation densities, and chemical potentials) are well-predicted by the CS-LDA. MD simulations do reveal oscillatory ion densities and chemical potentials due to steric repulsions between ions, which cannot be captured by any LDA model. Nonetheless, the CS-LDA accurately describe the diffuse portion of PM chemical potential profiles (Figures 1−3) and even captures the capacitance of the oscillatory (correlated) portions of PM EDLs. This has both positive and negative consequences: it implies that CS-LDA computations can be used to faithfully predict the capacitance of even moderately correlated EDLs, yet it also implies that measurements of integrated quantities (like capacitance) tend to mask oscillatory EDL structures. Attempts to extract detailed EDL profiles (or to test the suitability of LDAs) from measurements of such integrated quantities may therefore be misleading. As recently emphasized by Gillespie,[19] accurate models of the density profiles require local averages of ion concentrations that LDAs inherently neglect. While we did not consider them here, models that use locally averaged concentrations to determine excess chemical potentials due to the excluded volume may much better describe near-electrode effects.

While the present work has treated a fairly broad swath of parameter space, it does omit various physical effects that can play important roles in EDL structure and dynamics. Ion size asymmetries, for example, will clearly modify the details of the steric contributions to the excess chemical potential of co- and counterions in EDLs. Co-ions that are much smaller (or larger) than counterions will introduce a weaker (or stronger) steric penalty. Analogous chemical potentials for multiple hard-sphere sizes have been described by the Boublík, Mansoori, Carnahan, Starling, and Leland (BMCSL)[19,23,32,44] equation of state, and it would be interesting to analyze such effects in a manner analogous with this work. Moreover, we expect the structure of EDLs in electrolytes containing two or more species of counterions, each with a distinct size, valence, and/or charge specificity,[12] will differ considerably from the binary electrolytes studied here. Finally, this work has omitted any explicit treatment of the solvent, instead incorporating solvation shells in terms of an effective ion size. One could imagine modifying the current approach to treat solvent explicitly using the BMCSL, with (uncharged) solvent molecules of one size interacting with (charged) ions of a different size.

The present work reveals both the qualitative and quantitative consequences of finite ion sizes in the structure and properties of electric double layers and of the ability of various LDAs to account for finite ion size in predicting quantitative features of EDLs. We hope that our work establishes a framework for future studies that account for the additional physicochemical phenomena.

AUTHOR INFORMATION

Corresponding Author

*E-mail: squires@engineering.ucsb.edu.

Notes

The authors declare no competing financial interest.

ACKNOWLEDGMENTS

We gratefully acknowledge primary support from the U.S. Department of Energy through the Los Alamos National Laboratory/UCSB Institute for Multiscale Materials Studies and partial support from the W. M. Keck Foundation, the UCSB Doctoral Scholars Graduate Fellowship, and Lawrence Livemore National Laboratory under contract DE-AC52-07NA27344.

REFERENCES

(1) Russel, W. B.; Saville, D. A.; Schowalter, W. R. *Colloidal Dispersions*; Cambridge University Press: Cambridge, 1989.
(2) Vlachy, V. Ionic Effects beyond Poisson−Boltzmann Theory. *Annu. Rev. Phys. Chem.* **1999**, *50*, 145−165.
(3) Schoch, R. B.; Han, J.; Renaud, P. Transport Phenomena in Nanofluidics. *Rev. Mod. Phys.* **2008**, *80*, 839−883.
(4) Deryagin, B.; Dukhin, S. Theory of Surface Conductance. *Colloid J.* **1969**, *31*, 277.
(5) Brogioli, D. Extracting Renewable Energy from a Salinity Difference Using a Capacitor. *Phys. Rev. Lett.* **2009**, *103*, 058501.
(6) Conway, B. E. *Electrochemical Supercapacitors: Scientific Fundamentals and Technological Applications*; Plenum Publishers: New York, 1999.
(7) Fedorov, M., Kornyshev, A. Ionic Liquids at Electrified Interfaces *Chem. Rev.* **2014**.
(8) Luo, G.; Malkova, S.; Yoon, J.; Schultz, D.; Lin, B.; Meron, M.; Benjamin, I.; Vanýsek, P.; Schlossman, M. Ion Distributions Near a Liquid−Liquid Interface. *Science* **2006**, *311*, 216.
(9) Laanait, N.; Mihaylov, M.; Hou, B.; Yu, H.; Vanỳsek, P.; Meron, M.; Lin, B.; Benjamin, I.; Schlossman, M. L. Tuning Ion Correlations at an Electrified Soft Interface. *Proc. Natl. Acad. Sci. U.S.A.* **2012**, *109*, 20326−20331.
(10) Shapovalov, V. L.; Brezesinski, G. Breakdown of the Gouy−Chapman Model for Highly Charged Langmuir Monolayers: Counter-ion Size Effect. *J. Phys. Chem. B* **2006**, *110*, 10032−10040.
(11) Burt, R.; Birkett, G.; Zhao, X. S. A Review of Molecular Modeling of Electric Double Layer Capacitors. *Phys. Chem. Chem. Phys.* **2014**, 1−20.
(12) Huang, D. M.; Cottin-Bizonne, C.; Ybert, C.; Bocquet, L. Ion-Specific Anomalous Electrokinetic Effects in Hydrophobic Nano-channels. *Phys. Rev. Lett.* **2007**, *98*, 177801.
(13) Rica, R.; Ziano, R.; Salerno, D.; Mantegazza, F.; Brogioli, D. Thermodynamic Relation between Voltage−Concentration Depend-ence and Salt Adsorption in Electrochemical Cells. *Phys. Rev. Lett.* **2012**, *109*, 156103.
(14) Suss, M. E.; Biesheuvel, P.; Baumann, T. F.; Stadermann, M.; Santiago, J. G. In Situ Spatially and Temporally Resolved Measure-ments of Salt Concentration between Charging Porous Electrodes for Desalination by Capacitive Deionization. *Environ. Sci. Technol.* **2014**, *48*, 2008−2015.
(15) Mirzadeh, M.; Gibou, F. A Conservative Discretization of the Poisson−Nernst−Planck Equations on Adaptive Cartesian Grids. *J. Comput. Phys.* **2014**, *274*, 633−653.
(16) Gebbie, M.; Valtiner, M.; Banquy, X.; Fox, E.; Henderson, W.; Israelachvili, J. Ionic Liquids Behave as Dilute Electrolyte Solutions. *Proc. Natl. Acad. Sci. U.S.A.* **2013**, *110*, 9674−9679.
(17) Bazant, M. Z.; Kilic, M. S.; Storey, B. D.; Ajdari, A. Towards an Understanding of Induced-Charge Electrokinetics at Large Applied Voltages in Concentrated Solutions. *Adv. Colloid Interface Sci.* **2009**, *152*, 48−88.
(18) Israelachvili, J. N. *Intermolecular and Surface Forces*; Academic Press: London, 1992.
(19) Gillespie, D. A Review of Steric Interactions of Ions: Why Some Theories Succeed and Others Fail To Account for Ion Size. *Microfluid. Nanofluid.* **2014**, 1−22.
(20) di Caprio, D.; Borkowska, Z.; Stafiej, J. Specific Ionic Interactions within a Simple Extension of the Gouy−Chapman

DOI: 10.1021/la5048936
Langmuir XXXX, XXX, XXX−XXX

Theory Including Hard Sphere Effects. *J. Electroanal. Chem.* **2004**, *572*, 51−59.
(21) Bikerman, J. XXIX. Structure and Capacity of Electrical Double Layer. *Philos. Mag., Ser. 7* **1942**, *33*, 384−397.
(22) Kilic, M. S.; Bazant, M. Z.; Ajdari, A. Steric Effects in the Dynamics of Electrolytes at Large Applied Voltages. I. Double-Layer Charging. *Phys. Rev. E* **2007**, *75*, 021502.
(23) Biesheuvel, P.; van Soestbergen, M. Counterion Volume Effects in Mixed Electrical Double Layers. *J. Colloid Interface Sci.* **2007**, *316*, 490−499.
(24) Kornyshev, A. A. Double-Layer in Ionic Liquids: A Paradigm Change? *J. Phys. Chem. B* **2007**, *111*, 5545−5557.
(25) Giera, B.; Henson, N.; Kober, E. M.; Squires, T. M.; Shell, M. S. Model-Free Test of Local-Density Mean-Field Behavior in Electric Double Layers. *Phys. Rev. E* **2013**, *88*, 011301.
(26) Weeks, J. D.; Chandler, D.; Andersen, H. C. Role of Repulsive Forces in Determining the Equilibrium Structure of Simple Liquids. *J. Chem. Phys.* **1971**, *54*, 5237−5247.
(27) Carnahan, N. F.; Starling, K. E. Equation of State for Nonattracting Rigid Spheres. *J. Chem. Phys.* **1969**, *51*, 635−636.
(28) Attard, P. Electrolytes and the Electric Double Layer. *Adv. Chem. Phys.* **1996**, *92*, 1−160.
(29) Qiao, R.; Aluru, N. R. Ion Concentrations and Velocity Profiles in Nanochannel Electroosmotic Flows. *J. Chem. Phys.* **2003**, *118*, 4692−4701.
(30) Gouy, M. Sur la Constitution de la Charge Electronique a la Surface d'un Electrolyte. *J. Phys. Theor. Appl.* **1910**, *9*, 457−468.
(31) Chapman, D. L. A Contribution to the Theory of Electrocapillarity. *Philos. Mag., Ser. 6* **1913**, *25*, 475−481.
(32) Hansen, J.; McDonald, I. *Theory of Simple Liquids*; Academic Press: San Diego, CA, 1986.
(33) Barker, J.; Henderson, D. What Is "Liquid"? Understanding the States of Matter. *Rev. Mod. Phys.* **1976**, *48*, 587−671.
(34) Song, Y.; Mason, E.; Stratt, R. Why Does the Carnahan−Starling Equation Work So Well? *J. Phys. Chem.* **1989**, *93*, 6916−6919.
(35) McQuarrie, D. A. *Statistical Mechanics*; University Science Books: Sausalito, CA, 1976.
(36) Attard, P. Simulation of the Chemical Potential and the Cavity Free Energy of Dense Hard-Sphere Fluids. *J. Chem. Phys.* **1993**, *98*, 2225.
(37) Abraham, F. F.; Singh, Y. The Structure of a Hard-Sphere Fluid in Contact with a Soft Repulsive Wall. *J. Chem. Phys.* **1977**, *67*, 2384−2385.
(38) Plimpton, S. Fast Parallel Algorithms for Short-Range Molecular Dynamics. *J. Comput. Phys.* **1995**, *117*, 1−19.
(39) Schneider, T.; Stoll, E. Molecular-Dynamics Study of a Three-Dimensional One-Component Model for Distortive Phase Transitions. *Phys. Rev. B* **1978**, *17*, 1302−1322.
(40) Hockney, R.; Eastwood, J. *Computer Simulation Using Particles*; Taylor & Francis: New York, 1989.
(41) Widom, B. Structure of Interfaces from Uniformity of the Chemical Potential. *J. Stat. Phys.* **1978**, *19*, 563−574.
(42) Barker, J. A.; Henderson, D. Perturbation Theory and Equation of State For Fluids. II. A Successful Theory of Liquids. *J. Chem. Phys.* **1967**, *47*, 4714−4721.
(43) Levesque, D.; Verlet, L. Perturbation Theory and Equation of State for Fluids. *Phys. Rev.* **1969**, *182*, 307.
(44) Mansoori, G.; Carnahan, N.; Starling, K.; Leland, T. W., Jr. Equilibrium Thermodynamic Properties of the Mixture of Hard Spheres. *J. Chem. Phys.* **1971**, *54*, 1523.

DOI: 10.1021/la5048936
Langmuir XXXX, XXX, XXX−XXX